A&A manuscript no.
(will be inserted by hand later)

Your thesaurus codes are:
(07.36.1; 03.10.1; 09.09.1; 09.14.1)

ASTRONOMY
AND
ASTROPHYSICS
1.7.1994

Diffuse continuum gamma rays from the Galaxy observed by COMPTEL

A.W. Strong[1], K. Bennett [4], H. Bloemen [2*], R. Diehl [1], W. Hermsen [2], D. Morris [3], V. Schönfelder [1], J.G. Stacy [3], C. de Vries [2] M.Varendorff [1], C. Winkler [4], and G. Youssefi [1]

[1] Max-Planck Institut für extraterrestrische Physik, Giessenbachstrasse, Postfach 1603, 85740 Garching, FRG
[2] SRON-Leiden, P.B. 9504, NL-2300 RA Leiden, The Netherlands
[3] University of New Hampshire, Institute for the Study of Earth, Oceans and Space, Durham NH 03824, USA
[4] Astrophysics Division, ESTEC, 2200 AG Noordwijk, The Netherlands

[the date of receipt and acceptance should be inserted later]

Abstract. The diffuse Galactic continuum gamma-ray emission has been studied using the full Sky Survey from COMPTEL on the Compton Observatory CGRO. The diffuse emission appears to be visible in the whole 0.75-30 MeV range covered by the instrument, although a considerable contribution from unresolved point sources cannot be excluded. A correlation analysis using HI and CO surveys of the Galaxy is used to derive the Galactic emissivity spectrum, and this is consistent with a smooth continuation to the spectrum at higher energies derived by a similar analysis of COS-B data. The apparent conversion factor from integrated CO temperature to molecular hydrogen column density can also be determined from the correlation analysis. The value obtained is consistent with results from COS-B and other non-gamma-ray methods. Calculations of the emissivity spectrum from bremsstrahlung from a cosmic-ray electron spectrum based on propagation models are compared with the observations.

Key words: gamma rays: general; cosmic rays; interstellar medium :clouds: general; interstellar medium :general

1. Introduction

The diffuse continuum γ-ray emission from the Galactic plane at MeV energies is believed to originate mainly in bremsstrahlung interactions of cosmic-ray electrons with interstellar gas. Measurement of the γ-ray spectrum at low energies therefore provides important constraints on the spectrum and propagation of cosmic-ray electrons. This information is complementary to direct measurements and estimates based on radio synchrotron radiation. Together with cosmic-ray nuclear composition studies, the aim is to gain a consistent picture of cosmic-ray origin and propagation including such questions as the nature of the sources, the size of the propagation region (e.g. existence of a 'halo') and the rôles of diffusion and convection. Because of the large energy losses due to ionization, low energy electrons are especially sensitive to Galactic propagation effects. Energy losses are related to the gas distribution at low energies (ionization and bremsstrahlung) and to magnetic fields and radiation density (synchrotron and inverse-Compton emission) at high energies; it follows that the electron spectrum is sensitive to the spatial properties of the propagation process.

Gamma-ray studies have also made an important contribution to the study of the interstellar medium by providing an independent estimate of the scaling factor required to estimate molecular hydrogen column densities from ^{12}CO surveys. The first estimate from COS-B data (Lebrun et al. 1983) was refined in subsequent analysis (Bloemen et al. 1984,1986 , Strong et al. 1988) and has often been used by radio astronomers to derive masses from CO data (e.g. Bronfman et al. 1988).

Observations at MeV energies are difficult and until now have mainly been made with non-imaging detectors which give a wide-angle average of the emission to be measured. The COMPTEL instrument on the Compton Observatory has sufficient imaging capability to allow a sensitive measurement of the diffuse radiation. Preliminary mapping of the Galactic plane (see Bloemen et al. 1994) shows that the Galactic ridge can be detected; the energy spectrum of intensity may then be determined by model fitting. The present approach to COMPTEL data analysis has been largely influenced by that for the COS-B data (Bloemen et al. 1986, Strong et al. 1988); in that work it was found possible not only to separate the components of diffuse emission associated with atomic and molecular gas in the Galaxy, but also to determine the large-scale emissivity gradient. This gradient was found to be quite small, and has surprising consequences for the sources and propagation of cosmic rays (see Bloemen 1989, Bloemen 1993, Strong 1994 for reviews of this topic).

Using early parts of the COMPTEL Sky Survey preliminary results have been published (Strong et al. 1993a,b; Strong et al. 1994); now the entire Galactic plane is covered and this enlarged database forms the basis of the present paper.

The imaging Compton telescope COMPTEL is one of four instruments on board the Compton Gamma Ray Observatory satellite launched on April 5, 1991. COMPTEL operates in the 0.75 to 30 MeV range with a field of view of 1 steradian, a position location accuracy for bright sources of about 0.5^o ,

* Also Leiden Observatory

an energy resolution better than 10% FWHM and a sensitive area of about 40 cm^2 (Schönfelder et al. 1993).

2. Data and analysis method

2.1. COMPTEL Observations

The instrument is described in Schönfelder et al. (1993); an explanation of the response is given in Diehl et al. (1992). For each incident photon detected by the instrument, the energy deposits and interaction locations in the upper and lower detectors are measured. The Compton scatter angle $\bar{\varphi}$ is computed from the measured energy deposits, and the photons are binned in a 3-D dataspace consisting of the scatter direction (2 angles) and $\bar{\varphi}$. The binning used here is 1^o in scatter direction and 2^o in $\bar{\varphi}$. The response of the instrument in this dataspace to a given incident γ-ray intensity distribution is computed on the basis of the knowledge of the instrument configuration (as a function of time), the pre-launch calibration and simulations. Hence, given a parameterized model of the sky, the values of the parameters can be determined by model fitting in the dataspace described above.

Table 1a summarizes the 25 observations used in this work. All measured telescope events having scatter direction with $|b| < 35^o$ were used. The observations were combined by adding the counts and computing the effective response for the combined dataset.

Table 1a. Summary of COMPTEL Galactic plane observations used

Observation	Target	l	b
1	Crab	191^o	-5^o
2.0	Cyg X-1	73^o	$+3^o$
5	G. Centre	0^o	-4^o
6	SN1987A	278^o	-29^o
7.0	Cyg X-3	70^o	-8^o
7.5	Gal 025-14	25^o	-14^o
8	Vela PSR	263^o	-6^o
12	Cen A	311^o	$+22^o$
13.0	Gal 025-14	25.0^o	-14^o
14	Eta Car	285^o	-1^o
15	NGC1275	153^o	-13^o
16	Sco X-1	0^o	$+20^o$
17	SN1987A	283^o	-32^o
20	SS433	40^o	$+1^o$
23	Cir X-1	322^o	$+3^o$
27	4U1543-47	332^o	$+2^o$
30+33	NGC2992	252^o	$+31^o$
31	MCG+8-11-11	163^o	$+12^o$
32	NGC3783	284^o	$+23^o$
34	Cas A	109^o	-2^o
35+38	ESO141-55	335^o	-26^o
36.0+36.5	GRO J0422+32	169^o	-10^o
39	GRO J0422+32	168^o	-9^o
41+44	GAL 228+03	228^o	$+3^o$
43	MRK509	31^o	-28^o

Table 1b. Summary of COMPTEL high-latitude observations used to estimate the instrumental background

Observation	Target	l	b
4	NGC4151	156^o	$+72^o$
9.0	GAL339-84	338^o	-84^o
13.5	GAL339-84	338^o	-84^o
10	Fairall 9	287^o	-54^o
21	NGC1068	171^o	-53^o
24	GAL010+57	10^o	$+57^o$
25	GAL007+48	7^o	$+48^o$
40	MCG+5-23-16	195^o	$+44^o$

2.2. The model

We assume the continuum radiation originates in cosmic-ray interactions with interstellar gas, and therefore use the relation

$$I_\gamma = \frac{q}{4\pi}(N_{HI} + 2X_\gamma W_{CO}) + \Sigma I_s + I_B \quad (1)$$

where I_γ is the γ-ray intensity (cm^{-2} $sr^{-1}s^{-1}$), q the γ-ray emissivity per H atom, N_{HI} the atomic hydrogen gas column density and W_{CO} the integrated ^{12}CO temperature; I_s represents point sources included in the model (only the Crab in the present work) and I_B is an isotropic term. N_{HI} is based on a combination of various 21-cm surveys, and W_{CO} on the CO survey of Dame et al. (1987). The survey data is identical to that used by Strong et al. (1988) for the analysis of COS-B data and the reader is referred to that paper for further details. Unlike the COS-B analysis, no radial gradient is included yet since this is expected to have only a minor effect (only a small gradient was found from the COS-B data); the emissivity is then an average value appropriate to the location of greatest γ-ray emission, i.e. the inner Galaxy. We assume that the molecular hydrogen column density is related to the integrated CO temperature by $X_{CO} = N_{H_2}/W_{CO}$ but for the γ-ray analysis we represent the coefficient of W_{CO} by X_γ to make clear that it may differ from X_{CO} due (for example) to different cosmic-ray densities in clouds relative to the diffuse medium; X_γ can either be left as a free parameter or fixed at a value such as 2.3 10^{20} mols. cm^{-2} /(K km s^{-1}) as determined from COS-B data by Strong et al. (1988).

The free parameters of the model are q, X_γ , I_s (one parameter per source), I_B and the instrumental background level. Since the instrumental background is rather high and not known *a priori* its treatment is critical in obtaining a reliable result. We use high-latitude observations as the basis for our background estimates, assuming that the shape of this background is the same in the instrument system for all observations. To obtain a good estimate of the average background shape several high-latitude observations sources were summed in the instrument system and the resulting arrays interpolated to the coordinate system of the Galactic plane pointings using bi-cubic splines. The high-latitude observations used are summarized in Table 1b; they were chosen to have $|b| > 40^o$ and so that no strong point sources were within the field of the COMPTEL data. The *absolute* level of instrumental background was left free to be determined by the fitting procedure.

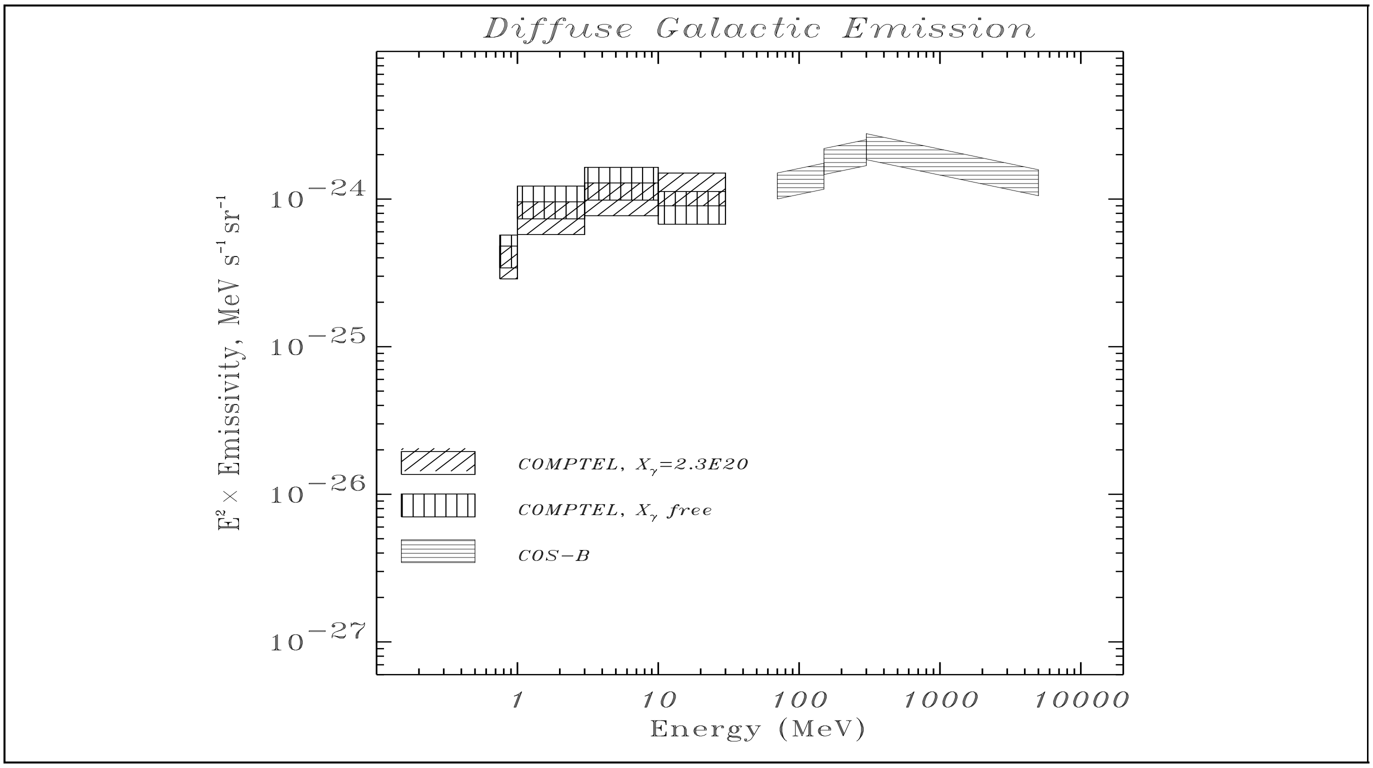

Fig. 1. Emissivity spectrum of the Galaxy derived from COMPTEL data together with values from a similar analysis of COS-B data (Strong et al. 1988). The COMPTEL spectrum is shown for both X_γ fixed at 2.3 10^{20} mols. cm^{-2} /(K km s^{-1}) and for X_γ free.

2.3. Instrument response and fitting method

The instrument response to a given intensity distribution I_γ can be expressed in the form

$$n(\boldsymbol{r}, \bar{\varphi}) = g(\boldsymbol{r}) \int_{\Omega} I_\gamma(\boldsymbol{r}')X(\boldsymbol{r}')f(\boldsymbol{r}, \boldsymbol{r}', \bar{\varphi})d\Omega' \qquad (2)$$

where n is the expected counts per bin of data space, $\boldsymbol{r}$ is the measured scatter direction of the γ-ray , Ω is the solid angle on the celestial sphere, $\boldsymbol{r}'$ is the incoming direction, X($\boldsymbol{r}'$) is the exposure of the D1 modules to the incoming radiation (in cm^{2}s), $g(\boldsymbol{r})$ is a geometrical factor determined by the spatial arrangement of the D1 and D2 modules, $f(\boldsymbol{r}, \boldsymbol{r}', \bar{\varphi})$ is a point-spread-function (PSF) giving the probability that a photon arriving at D1 interacts there and scatters from $\boldsymbol{r}'$ to $\boldsymbol{r}$ and has a measured Compton scatter angle $\bar{\varphi}$. Since in practice the data are binned in energy ranges, Eq(2) has to be integrated over energy using an assumed spectral form for I_γ; this is taken to be a power-law with index -2.0 in the present analysis. The response is rather insensitive to the precise spectrum assumed, but it is necessary to check for consistency with the spectrum derived by the fitting procedure. The calculation of the PSF for a given spectrum and energy range makes use of the prelaunch calibration (Schönfelder et al. 1993) and can be derived using an analytical model of the response or by direct simulation of γ-rays passing through the instrument. Since the PSF is our main source of uncertainty in deriving absolute fluxes, both methods have been used; differences indicate the size of systematic errors due to the PSF.

We use the likelihood ratio method to fit the model to the data using the full instrument response; the use of Poisson statistics means that the binning can be made arbitrarily small and in fact the adopted values are determined by computational constraints only. The errors on the parameters are estimated by the method described by Strong (1985a) which approximates the log-likelihood ratio in the parameter space by a quadratic function and uses the known distribution of this statistic to obtain a confidence interval for each parameter properly taking into account the uncertainty in all parameters. The statistical errors are quoted for a log-likelihood ratio of 0.5 corresponding to 68% (1σ) confidence intervals. The uncertainty is however dominated by systematic errors, estimated to be of order 25% and the latter value has been used in plotting the emissivity spectra.

3. Results of fitting procedure

3.1. Overview of fit results

Table 2 summarizes the results of the fits to Eq. (1) in the four standard COMPTEL energy ranges. The Crab was included as the only point source, with a flux determined by the fitting. Two cases are considered: X_γ fixed at 2.3 10^{20} mols. cm^{-2} /(K km s^{-1}) , and X_γ free. The fit to Eq.(1) gives significant determinations of both q and X_γ for all energy ranges: we may conclude that the Galactic continuum radiation was indeed detected, that the emissivities can confidently be interpreted in terms of emission from the interstellar medium and that the components associated with HI and H_2 can be separated on the basis of their different angular distibutions. For the case where X_γ is free the *error weighted* average X_γ over the four energy bands is $1.26\pm.3\ 10^{20}$ mols. cm^{-2} /(K km s^{-1}) and the unweighted average is 1.7 10^{20} mols. cm^{-2} /(K km s^{-1}) ; this is marginally consistent with the COS-B result at higher energies (see detailed discussion in Section 3.5). The emissivity spectrum is rather insensitive to whether we leave X_γ free or not, since it is constrained by the HI component as well (see Eq.(1)). From the counts per component given in Table 2 about 15% of the Galactic emission below 10 MeV is attributed to H_2, the rest to HI. In the 10-30 MeV range, using the fitted X_γ value, the H_2 contribution is larger: about 30%. The relatively small H_2 contribution to the total counts is attributable to the much wider latitude and longitude distribution of the HI relative to H_2.

The question of the contribution from point sources which may lead to inaccurate results from the model fitting can be addressed partly by noting that the counts from the Crab (the only source explicitly included in the model) are about 10% of the total diffuse signal from the Galactic plane (see Table 2). Since the Crab is by a large factor the brightest source in the COMPTEL energy range, it is unlikely that a large contribution comes from further *detectable* point-sources. A contribution from many unresolved sources cannot be excluded, just as in the COS-B case; a more detailed analysis requires modelling populations of sources, which is beyond the scope of the present work.

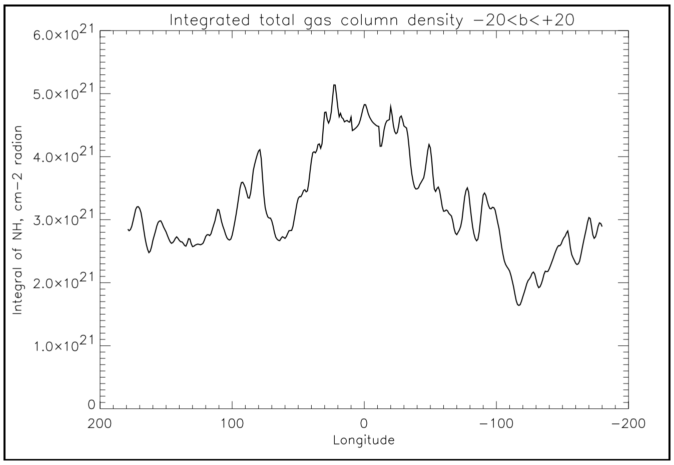

Fig. 2. Total gas column density (HI and H_2) from 21-cm and CO surveys integrated over -20^o <b<+20^o

3.2. Comparison with other experiments

In order to compare with other experimental results for the Galactic centre region, where the results are normally given as a flux per radian integrated over latitude, we use, for the COMPTEL and COS-B intensities, the quantity

$$J_\gamma = \frac{q}{4\pi} \int_{-20^o}^{+20^o} N_H db \qquad (3)$$

averaged over -30^o <l<+30^o . Fig 2 shows the longitude dependence of $\int_{-20^o}^{+20^o} N_H db$ for reference. Fig 3 gives a compilation of results for the flux in the inner Galaxy; note that such a comparison is at best approximate because of the very different angular responses of the various instruments and the fact that the observations refer to different regions of the (inner) Galactic plane. In any case the COMPTEL result is consistent with the overall picture from other instruments. The difficulty of comparison underlines the need for a uniform analysis method for different instruments; note that the approach used here could be applied to data from other instruments and this would allow direct comparison of results (as is the case for the COMPTEL and COS-B analysis shown in Fig 1).

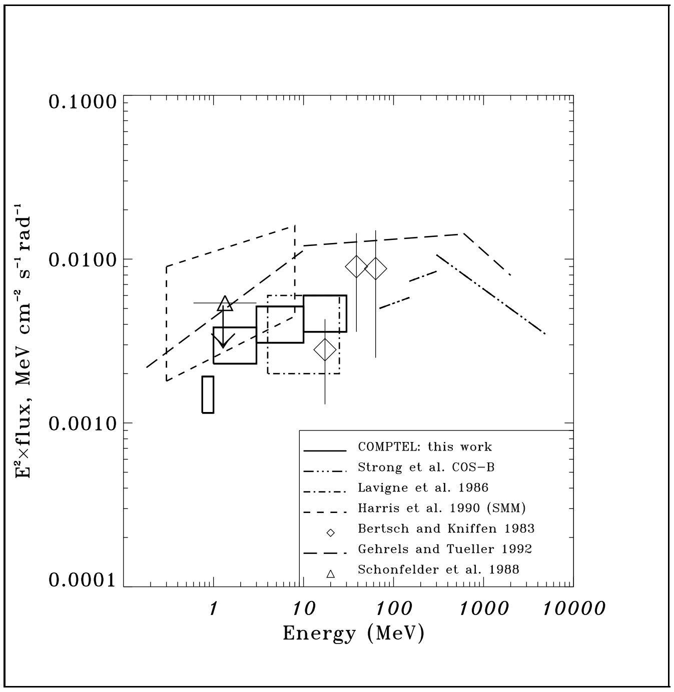

Fig. 3. Compilation of flux measurements for inner Galaxy. Fluxes are integrated over latitude as described in the text. For clarity COMPTEL points are shown only for X_γ =2.3 10^{20} mols. cm^{-2} /(K km s^{-1})

3.3. Validity of the model

The analysis presented so far has been purely statistical: we have assumed a particular model and obtained the best-fitting parameters for our data. We can now ask whether the model is a valid one to use; in particular does it provide a satisfactory fit to the data, and is it supported by the data ? It has to be pointed out immediately that for COMPTEL data, because of their complex 3 dimensional data space, *direct* comparison of the model with an image of the sky is rather difficult. Images are obtained by maximum-entropy deconvolution methods (Strong et al. 1992); these are model-free but are limited by the relatively low signal-to-noise due to the high background level, this limitation being particularly important when dealing with *extended, diffuse* emission. Fig 4 (upper) shows a maximum-entropy image of the Galactic plane in the 1-3 MeV range. The Galactic plane is clearly detected, as has been previously

Table 2. Results of model fitting (equation (1)) to COMPTEL data. Errors are 1σ and statistical only.

MODEL PSF

Energy range (MeV)	0.75-1.0	1.0-3.0	3.0-10.0	10.0-30.0
X_γ fixed at 2.3 10^{20} mols. cm^{-2} /(K km s^{-1})				
$q/4\pi$ ($10^{-25} sr^{-1} s^{-1}$)	1.28±.09	5.1 ±.11	2.4±.07	0.85±.027
X_γ (10^{20} mols. cm^{-2} /(K km s^{-1}))	(2.3)	(2.3)	(2.3)	(2.3)
Crab flux (10^{-4}cm^{-2}s^{-1})	4.2	10.9	3.4	0.96
Counts from HI+CO components	32409	202987	69665	15611
Counts from Crab	5886	24618	5786	1011
Relative log-likelihood	-54140	5552056	1402268	-167055
X_γ free				
$q/4\pi$ ($10^{-25} sr^{-1} s^{-1}$)	1.52±.17	6.53±.22	3.06±.14	0.73±.05
X_γ (10^{20} mols. cm^{-2} /(K km s^{-1}))	1.60±.35	1.13±.11	1.13±.16	3.0±.46
Crab flux(10^{-4}cm^{-2}s^{-1})	3.9	10.4	3.3	0.93
Counts from HI component	29141	196701	68147	10409
Counts from CO component	6257	31901	10511	4320
Counts from Crab	5794	23453	5488	1030
Total counts	561438	4225569	1927835	351225
Relative log-likelihood	-54139	5552095	1402284	-167054

SIMULATED PSF

Energy range (MeV)		1.0-3.0	3.0-10.0	10.0-30.0
X_γ fixed at 2.3 10^{20} mols. cm^{-2} /(K km s^{-1})				
$q/4\pi$ ($10^{-25} sr^{-1} s^{-1}$)		5.3 ±.12	2.25±.07	0.80±.03
X_γ (10^{20} mols. cm^{-2} /(K km s^{-1}))		(2.3)	(2.3)	(2.3)
Crab flux (10^{-4}cm^{-2}s^{-1})		11.5	2.9	1.05
Counts from HI+CO components		209269	72453	14388
Counts from Crab		25780	6137	1095
Relative log-likelihood		5551975	1402025	-166705
X_γ free				
$q/4\pi$ ($10^{-25} sr^{-1} s^{-1}$)		6.70±.26	2.90±.13	0.60±.05
X_γ (10^{20} mols. cm^{-2} /(K km s^{-1}))		1.37±.13	1.11±.16	4.31±.60
Crab flux (10^{-4}cm^{-2}s^{-1})		11.83	3.07	1.09
Counts from HI component		186506	71207	7891
Counts from CO component		36359	10904	4734
Counts from Crab		24689	5804	1144
Total counts		4225569	1927835	351225
Relative log-likelihood		5551980	1402044	-166695

shown, based on early COMPTEL observations, by Bloemen et al. (1994). We now wish to test whether the image we obtain is consistent with that which we should obtain if our adopted model based on gas tracers is valid. To this end we use a simulated dataset based on the model (with the fitted parameters) and the COMPTEL response; this dataset is input to the same maximum-entropy reconstruction procedure as for the real data and the resulting image is shown in Fig 4 (lower). The general similarity of the images is evident from visual inspection alone, demonstrating that the model is a plausible one. Differences in detail may be attributed at least partly to the inadequate background model. A more quantitative comparison of these results using latitude profiles of the image and simulation for the inner Galaxy (320^o <l<40^o) (Fig 5) indicates that they are compatible, although both are broader than the original model profile (also shown), due at least in part to the limitations of the deconvolution process mentioned above.

In contrast to the difficulty of comparison in *image space*, in the COMPTEL *data space* it is more straightforward. A comparison of predicted and observed counts for volume elements of the 3D data cube for 1-3 MeV is shown in Fig 6. The estimated data-space background has been subtracted in each case to show the 'signal' counts only. The linear correlation shows that the model indeed reproduces the data, although the scatter is clearly much above statistical, mainly due to the deficiencies in the background model. The linear correlation does not however rule out the possibility that models with other components would also fit the data, as suggested by the model-free

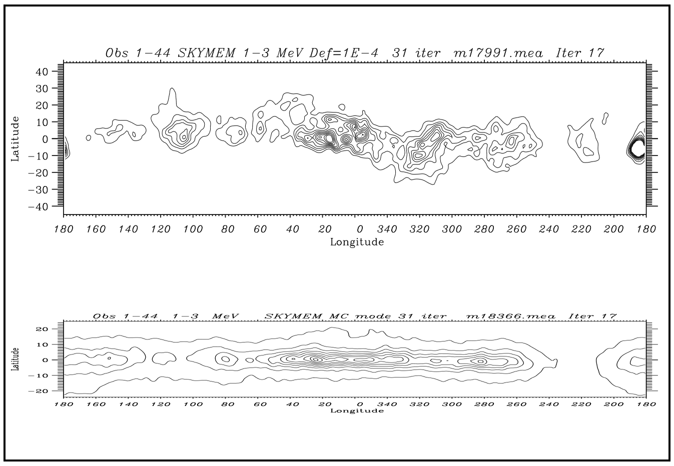

Fig. 4. Maximum-entropy image of the Galactic plane for 1-3 MeV based on COMPTEL data (top) compared with a maximum-entropy image generated from simulated data based on the gas model and the COMPTEL response. Note that the (l,b) scales are the same although the simulation is less extensive in b.

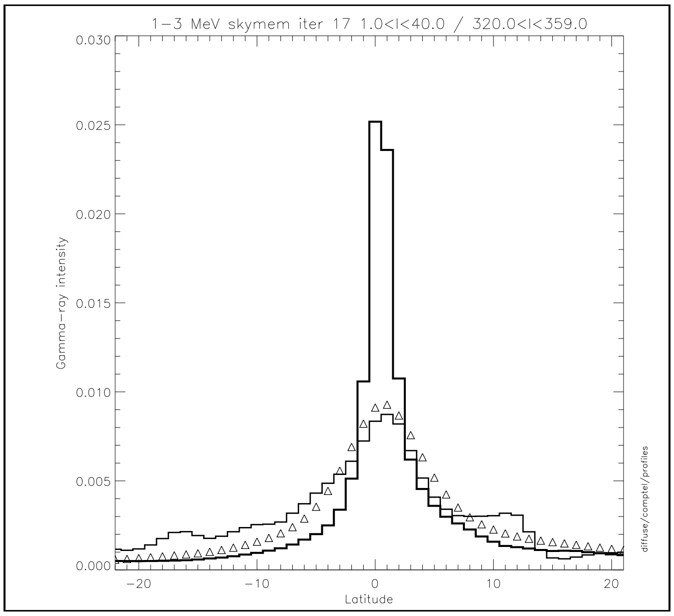

Fig. 5. Latitude profiles of maximum-entropy images for 1-3 MeV for 340^o <l<40^o . Lower histogram: using COMPTEL data; triangles: using simulated data based on gas model and COMPTEL response; upper histogram: original model (no reconstruction).

images discussed above. We cannot exclude that such components with a broader or more clumpy distribution than the gas model are present, and indeed some such contribution seems probable (see Bloemen et al. 1994); nevertheless our results demonstrate that *the model adopted in the present analysis is a reasonable first approach to interpreting the diffuse Galactic emission observed by COMPTEL.*

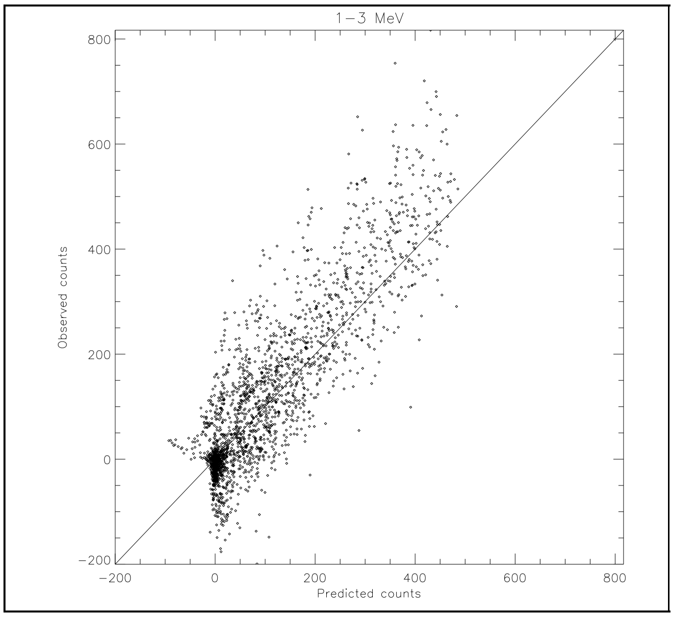

Fig. 6. Scatter plot of observed vs. predicted counts in COMPTEL dataspace for 1-3 MeV. The predicted counts are based on the gas model and the COMPTEL response. To increase the dynamic range of the plot the expected background counts have been subtracted on both axes.

3.4. The γ-ray emissivity spectrum

Fig 1 shows the emissivity spectrum of the Galaxy based on the present results. The likelihood values indicate that the model PSF is a better choice for the three lower energy ranges, and the simulated better for 10-30 MeV; hence these are the emissivities plotted in Fig 1. Both the spectra with X_γ fixed at 2.3 10^{20} mols. cm^{-2} /(K km s^{-1}) and with X_γ free are shown. The COMPTEL points are consistent with a spectral index of -2.0 and this slope is used to convert the values for each energy range to a differential spectrum in this plot. Errors on the COMPTEL points are estimated to be about 25%, including statistical and systematic errors. Also shown are values obtained from the application of a similar method, fitting COS-B data to the same gas model (Strong et al. 1988). The spectrum is consistent with a smooth connection to the COS-B spectrum. The COS-B values plotted are for the Solar galactocentric radius $R_\odot$; the inner Galaxy values are higher by about 50% due the to galactocentric gradient. Strictly all these emissivities represent upper limits since there may be some contribution from point sources in the Galactic plane.

3.5. γ-ray properties of molecular clouds

COMPTEL can clearly distinguish the γ-ray emission related to atomic and molecular hydrogen as traced by CO; this is possible because of the very different longitude and latitude distributions of these components. The X_γ parameter is therefore constrained by the γ-ray data; Fig 7 shows the measured X_γ for the energy ranges of the present analysis, together with results from COS-B (Strong et al. 1988). The COS-B fits also included a small radial variation in q, but this has a marginal effect on the X_γ values. The COS-B fit used here is for the case of energy-dependent X_γ and energy-independent gradient

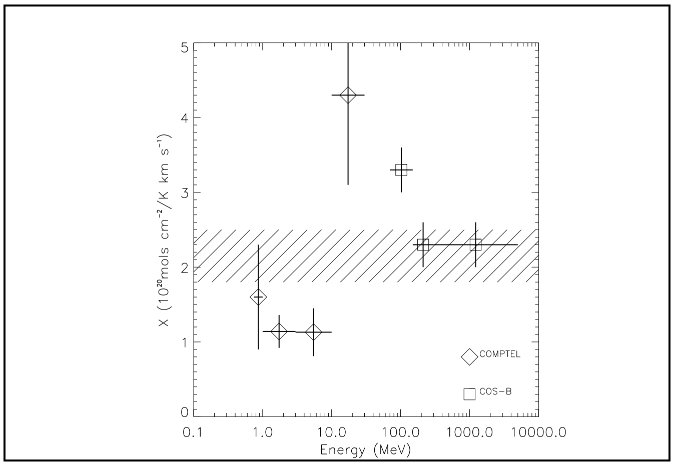

Fig. 7. Values of X_γ derived from γ-ray analyses in different energy ranges. The values below 30 MeV (diamonds) are from COMPTEL (present work) with 2σ error bars to allow for systematic effects; values above 70 MeV (squares) are from COS-B (Strong et al. 1988) using an identical analysis technique. The shaded area represents the range of values found by the application of the virial theorem to clouds.

since this was considered to give the best interpretation of the data.

We note first that the average X_γ from COMPTEL is marginally consistent within the errors with the COS-B value for E>150 MeV, 2.3±0.3 10^{20}. An energy-independent value of 2 10^{20} mols. cm^{-2} /(K km s^{-1}) over the 1 MeV - 1 GeV range would be an acceptable first approximation. However the COS-B data indicated that the situation is not so simple, with a higher X_γ in the 70-150 MeV range compared to E>150 MeV. The COMPTEL results also indicate an energy-dependence, with lower values than from COS-B below 10 MeV. Also there is an indication (but note the large error-bar !) of a higher value in the 10-30 MeV range, consistent with the value for the adjacent 70-150 MeV range from COS-B. Taken together, there seems to be some evidence for a peak in X_γ in the 10-100 MeV range.

The measured X_γ values are combinations of the 'true' average conversion factor X_{CO} and the γ-ray emissivity of molecular clouds relative to the atomic hydrogen component of the interstellar medium. If X_{CO} could be determined reliably by non- γ-ray methods then we could obtain information on the absolute emissivity of clouds. Recent X_{CO} values based mainly on application of the virial theorem to giant molecular clouds (Solomon et al. 1987, Lee et al. 1990, Sodroski 1991, Wolfire et al. 1993, Issa et al. 1990) give values of X_{CO} for the *inner* Galaxy in the range 1.6-2.8 10^{20} mols. cm^{-2} /(K km s^{-1}) and this is supported by infrared survey data (Kent et al. 1991). Values for the *outer* Galaxy (Digel et al. 1990, Carpenter et al. 1990, Sodroski 1991) tend to be significantly higher, but for the present analysis the inner Galaxy value is more relevant (see Strong 1994 for a summary table on this topic). On this basis we may *tentatively* conclude that there is some deficit in the emissivity of clouds relative to HI below 10 MeV, a slight enhancement in the 10-100 MeV range, while for E> 100 MeV the cloud emissivity is not detectably different from that of HI. Confirmation of these trends must await inclusion in the analysis of the large body of data following the initial COMPTEL Sky Survey.

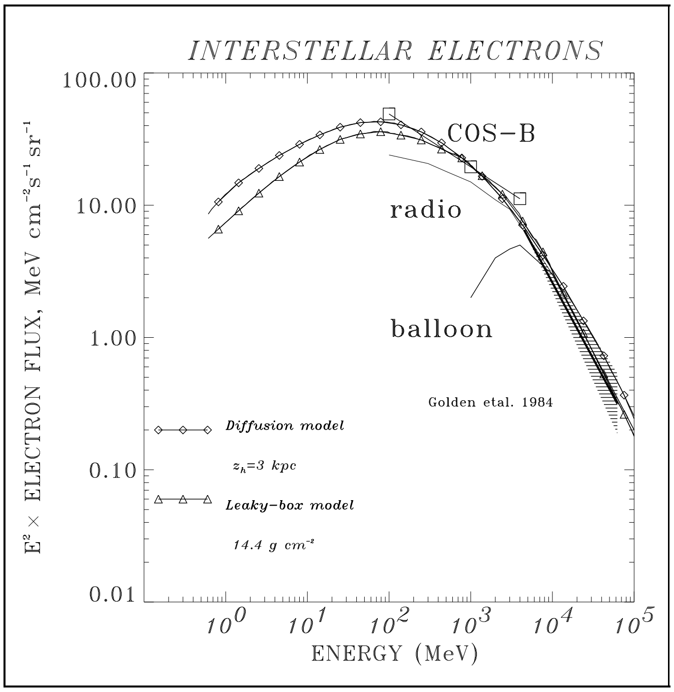

Fig. 8. Electron spectrum: horizontal shading: balloon measurement (Golden et al. 1984); continuous lines: balloon measurements (showing effect of solar modulation) and extrapolation based on radio observations (Webber 1983); squares: derived from COS-B γ-rays (Strong 1985b); diamonds: diffusive energy loss model with z_h=3 kpc, D=3 10^{28} cm^2 s^{-1} (spectrum at z = 0); triangles: leaky-box model with λ=14.4g cm^{-2} .

4. Discussion

4.1. Spectrum of cosmic-ray electrons

The low-energy interstellar electron spectrum is not directly measurable (due to solar modulation); the directly measured and demodulated spectrum above 1 GeV can be extrapolated down to about 200 MeV using the radio synchrotron spectrum (Webber 1983); further extrapolation to lower energies was earlier based on γ-ray upper limits (Sacher and Schönfelder 1984) or on propagation models (Webber 1983, Ip and Axford 1985). Fig 8 shows direct measurements above 1 GeV (Golden et al. 1984), an extrapolation based on radio observations (Webber 1983) and a spectrum in the 100-1000 MeV range based on COS-B (Strong 1985b). With the new emissivity spectrum shown in Fig 1, covering the 1 MeV -1 GeV range, we can re-evaluate the electron spectrum. Since we cannot directly deconvolve the bremsstrahlung spectrum to obtain the corresponding electron spectrum, the best way to proceed is to compute plausible model spectra based on propagation/energy loss models and compare the resulting bremsstrahlung emission with the observations. Spectra for the homogeneous ('leaky-box') model of cosmic-ray propagation have been calculated by Skibo and Ramaty (1993a,b,c), Skibo (1993), and Strong et al. (1993a,b) for particular choices of model parameters. Recently calculations using a more realistic (1-D) diffusive halo

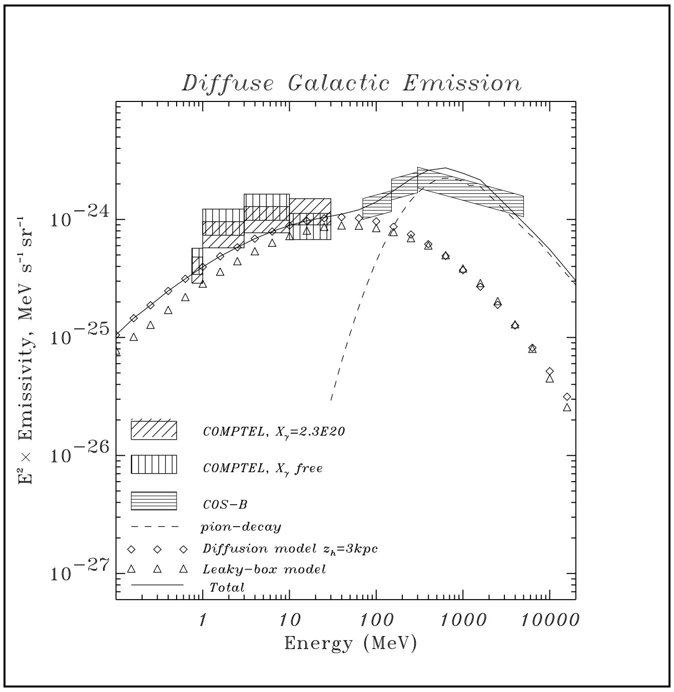

Fig. 9. Predicted γ-ray emissivity from bremsstrahlung based on computed electron spectra (from Fig 8) compared with COMPTEL and COS-B results. Diamonds: diffusive energy loss model with z_h=3 kpc, D=3 10^{28} cm^2 s^{-1} ; triangles: leaky-box model with λ=14.4g cm^{-2} . The solid line is the sum of bremsstrahlung and π^o-decay emission.

model have been undertaken (Strong and Youssefi 1994) and these will be used here. The π^o-decay emissivity is taken from Dermer (1986).

The low-energy electron spectrum is strongly modulated by ionization losses, so that the computed spectrum depends critically on the propagation parameters. Recent work on the cosmic-ray B/C abundance ratio, taking into account reactions with He and energy losses on ionized H in the ISM, indicates higher values of grammage (λ) than the conventional 6 - 8 g cm^{-2} . Soutoul et al. (1990) and Ferrando et al. (1991) give λ=14.4β g cm^{-2} below a few GV; for a critical discussion see Ferrando (1993). We use a 1-D diffusive halo model with parameters chosen to be consistent with this higher grammage: a half-thickness z_h=3 kpc at which height electrons escape freely, a diffusion coefficent D = 3 10^{28} cm^2 s^{-1} below 4 GeV and increasing as $E^{0.6}$ at higher energies (Bloemen et al. 1993b; Webber et al. 1992; Lukasiak et al. 1993). We adopt the measured distribution of HI (Dickey and Lockman 1990) and H_2 (via CO) in the Galaxy (Bronfman et al. 1988), and the extensive warm ionized medium (Reynolds 1993), allowing for an additional 1/9 by number of He. The grammage including He is given by $\lambda = \frac{13}{9} m_p z_h N_H/2D$ (see Bloemen et al. 1993b), where m_p is the proton mass and N_H is sum of the full disk vertical column densities of hydrogen in form of HI , H_2 and HII for which we use the values (6.7, 4.8, 1.0)$\times$ 10^{20} atoms cm^{-2} respectively. Inverse-Compton and synchrotron losses are included: these are important above 1 GeV. The electron injection spectrum is assumed to be a power-law with index -2.4. The interstellar spectrum is normalized at 1 GeV to the value derived from an a analysis of COS-B data (Strong 1985b): I_e(1 GeV) = 2 10^{-5} electrons cm^{-2}sr^{-1} s^{-1} MeV^{-1}. The resulting electron spectrum (at z = 0) is shown in Fig 8. For comparison, a leaky-box calculation with the same grammage is also shown: the diffusion model gives somewhat higher fluxes at low energies.

The computed bremsstrahlung emissivity spectrum spectrum per H atom in the Galactic plane (again allowing for the presence of He) is shown in Fig 9. It lies below the COMPTEL observed spectrum at least in the range 1-10 MeV. The fit would improve somewhat if a cosmic-ray gradient were included since this will tend to reduce the emissivities at R=R$_\odot$ in the COMPTEL range; this will be investigated in future work. The excess above the expected emission could indicate either a steepening of the electron injection spectrum at low energies or some additional γ-ray component such as point sources. As pointed out above, the latter is quite likely. Another possibility is inverse-Compton emission; calculations (Youssefi and Strong 1991) show that the contribution at a few MeV may well be significant; we intend to include this component explicitly in future studies.

The determination of the low-energy electron spectrum has interesting consequences. First, the large energy input to the interstellar medium via ionization may make an important contribution to the maintenance of the warm ionized medium (Chi and Wolfendale 1991; Skibo and Ramaty 1993 a,b,c); second that the *injection* spectrum of cosmic-ray electrons contains significant power compared to that of (relativistic) cosmic-ray nuclei even though the *ambient* electron spectrum has only a few percent of the energy content of the nuclei. This may have interesting consequences for theories of cosmic-ray origin.

4.2. Implications for cosmic-ray physics in clouds

If the energy-dependence of X_γ (Sec. 3.5) is real, there are various possible physical interpretations based on theoretical ideas from cosmic-ray physics. These are based on the fact that cosmic-ray electrons do not necessarily propagate freely into and out of clouds, and this affects their γ-ray emission in a variety of possible ways. Skilling and Strong (1976) investigated one mechanism for self-exclusion of cosmic ray nuclei: primary nucleons (1 MeV - 1 GeV) entering the cloud set up a gradient due to ionization losses, which leads to the generation of waves which scatter the particles and inhibit free entrance. This idea was extended to electrons by Strong and Skilling (1977): low energy electrons are scattered by waves produced by nucleons of the same momentum, excluding primary electrons and trapping secondaries. Further investigation by Morfill (1982) included the effects of particle acceleration by the converging Alfvén waves and also knock-on secondary electrons from nucleons which are an additional source at low energies. These processes only work up to $E_e \approx 300$ MeV since this corresponds to 50 MeV proton momentum where ionization losses become too small to drive the gradients causing the waves. It is therefore tempting to speculate that the decrease in X_γ at low energies may be understood in terms of exclusion of primary electrons from clouds, and that perhaps the peak at 100 MeV derives from secondary production and acceleration. More recently Dogiel and Sharov (1990) have studied acceleration by turbulence in clouds and made predictions of the γ-ray emission. More theoretical studies are clearly needed, and it is hoped they will be stimulated by the present results.

5. CONCLUSIONS

We have shown that COMPTEL can detect the low-energy continuum emission from the Galactic plane and measure its spectrum; the feasibility of separating the atomic and molecular gas components of the emission has also been demonstrated. These results represent a considerable step forward relative to measurements by previous instruments. The emissivity spectrum is approximately as expected for the simple case of a power-law electron injection spectrum modulated by ionization losses and with propagation parameters deduced from cosmic-ray composition, but with an indication that the observed emissivities are somewhat larger than expected; however the theoretical spectrum is very sensitive to the propagation parameters and further theoretical work is required on the interpretation. The excess in the MeV region could well be explained if point-sources or inverse-Compton emission make a significant contribution to the emission; this possibility must be investigated in future analysis of these and forthcoming data.

The detection of the molecular gas component and the determination of X_γ at low energies is a new result made possible by the use of the entire Galactic plane survey; the accuracy of the results is still limited, however, so these results should not be over-interpreted. Nevertheless the trend is in line with expectations based on basic physical processes, so this should be the starting point for further experimental and theoretical studies. Combination of these results with complementary data from the Compton Observatory OSSE and EGRET instruments will then be a very important next step in unravelling the components of the diffuse γ-ray emission from the Galaxy.

Acknowledgement This work was supported by NASA under contract NAS5-26645, by the German government through DARA under the grant 50 QV 9096 and by the Netherlands Organization for Scientific Research NWO.

REFERENCES

Bertsch, D.L., Kniffen D.A., 1983, ApJ **270**, 305
Bertsch, D.L. et al. 1993, ApJ **416**, 587
Bloemen, H. 1989, Ann. Rev. Astron. Astrophys. **27**, 469
Bloemen, H. 1993, in 'Back to the Galaxy', Holt, S.S., Verter, F. (eds), (New York) AIP Conf. Proc. **278**, 409
Bloemen, H. et al. 1984, A&A **135**, 12
Bloemen, H. et al. 1986, A&A, **154**, 25
Bloemen, H. et al. 1994, ApJ Supp., **92**, 419
Bloemen, H., Dogiel, V.A., Dorman, V.L., Ptuskin, V.S. 1993b, A&A, **267**, 372
Bronfman, L. et al. 1988, ApJ, **324**, 248
Carpenter, J.M., Snell, R.L., Schloerb, F.P. 1990, ApJ, 1990, **362**, 147
Chi, X., Wolfendale A.W. (1991) in 'The Interstellar Disk-Halo Connection in Galaxies', H. Bloemen (ed), IAU Symposium **144**, 197
Dame, T.M. et al., 1987, ApJ, **322**, 706
den Herder, J.W. et al., 1992, in 'Data Analysis in Astronomy IV', V. Di Gesù et al. (eds), Plenum Press, 217
Dermer, C.D. 1986, A&A, **157**, 223
Dickey, J.M., Lockman, F.J., 1990, Ann. Rev, Astron. Astrophys. **28**, 215
Diehl, R.D. et al., 1992, in 'Data Analysis in Astronomy IV', V. Di Gesù et al. (eds), Plenum Press, 201
Digel, S., Bally, J., Thaddeus, P. 1990, ApJ, **357**, L29
Dogiel, V. A., Sharov G. S. 1990, A&A, **229**, 259
Ferrando, P. et al., 1991, A&A, **247**, 163
Ferrando, P. 1993, Rapporteur paper, 23rd ICRC, Calgary
Gehrels, N., Tueller, J. 1993 , ApJ, **407**, 597
Golden, R.L. et al. 1984, ApJ, **287**, 622
Harris, M.J. et al., 1990, ApJ **362**, 135
Ip W.-H., Axford, W.I., 1985, A&A **149**, 7
Issa, M., Maclaren, I., Wolfendale A.W. 1990, ApJ, **352**, 132
Kent, S.M., Dame, T.M., Fazio G., 1991, ApJ **378**, 131
Lavigne, J.M. et al., 1986, ApJ **308**, 370
Lebrun, F. et al. 1983, ApJ, **274**, 231
Lee, Y., Snell, R.L., Dickman, R.L. 1990, ApJ, **355**, 536
Lukasiak, A. et al. 1993, Proc. 23rd ICRC, Calgary, **1**, 523
Morfill, G.E. 1982, ApJ, **262**, 749
Reynolds, R.J. 1993, in 'Back to the Galaxy', Holt, S.S., Verter, F. (eds), (New York) AIP Conf. Proc. **278**, 156
Sacher, W., Schönfelder, V., 1984, ApJ **279**, 817
Schönfelder, V., von Ballmoos, P., Diehl, R., 1988, ApJ **335**, 748
Schönfelder,V. et al., 1993, ApJ Supp. **86**, 657
Skibo, J.G. 1993, Ph.D. Dissertion, Univ. Maryland
Skibo, J.G., Ramaty. R. 1993a, A&A Suppl., **97,145**
Skibo, J.G., Ramaty. R. 1993b, in 'Compton Gamma Ray Observatory', St. Louis, AIP Conf. Proceedings **280**, 70
Skibo, J.G., Ramaty. R. 1993c, Proc. 23rd ICRC, Calgary, **2**, 132
Skilling, J., Strong, A.W. 1976, A&A, **53**, 253
Sodroski, T.J. 1991, ApJ, **366**, 95
Solomon, P.M. et al. 1987, ApJ, **319**, 730
Solomon. P.M., Barrett. J.W., 1991, in IAU Symp. 146, Combes, F., Casoli, F., (eds), 235
Soutoul, A., Ferrando P., Webber W.R. 1990, Proc. 21st ICRC, Adelaide, **3**, 337
Strong, A. W., 1985a, A&A, **150**, 273
Strong, A. W., 1985b, Proc. 19th ICRC, La Jolla, **1**, 333
Strong, A. W. 1994, Proc. 2nd Compton Symposium, Washington, AIP Conf. Proceedings **304**, 463
Strong, A. W. et al. 1992, in 'Data Analysis in Astronomy IV', ed. Di Gesù V. et al., Plenum Press, New York, p. 251
Strong, A. W., Skilling, J. 1977, ESA SP-124, 147
Strong, A. W. et al. 1988, A&A, **207**, 1
Strong, A. W. et al. 1993a, in 'Compton Gamma Ray Observatory', St. Louis, AIP Conf. Proceedings **280**, 35
Strong, A. W. et al. 1993b, Proc. 23rd ICRC, Calgary, **1**, 132
Strong, A. W. et al. 1994, ApJ Supp., **92**, 425
Strong, A.W., Youssefi G, 1994 (in preparation)
Solomon, P.M. et al. 1987, ApJ, **319**, 730
Webber, W.R. 1983, in 'Composition of Origin of Cosmic Rays', ed. Shapiro, M. M., pub. D. Reidel, p. 83
Webber, W.R., Lee, M.A., Gupta, M. 1992, ApJ, **390**, 96
Wolfire, M.G., Hollenbach, D., Tielens, A.G.G.M. 1993, ApJ **402**, 195
Youssefi, G., Strong, A. W. 1991, Proc. 22nd Int, Cosmic Ray Conf, Dublin, **1**, 129